Polym. Bull. (2018) 75:1563–1578
https://doi.org/10.1007/s00289-017-2112-1

ORIGINAL PAPER

$CoCl_2$-doped polyaniline composites as electrode materials with enhanced electrochemical performance for supercapacitor application

Malati Majhi[1] · R. B. Choudhary[1] · Anukul K. Thakur[1] · Fatin Saiha Omar[2] · Navaneethan Duraisamy[2] · Kasi Ramesh[2] · Subramaniam Ramesh[2]

Received: 19 November 2016 / Revised: 13 May 2017 / Accepted: 1 July 2017 /
Published online: 6 July 2017

Abstract HCl-doped polyaniline (PANI) and polymeric composites of polyaniline–cobalt chloride (PANI–$CoCl_2$) were synthesized in the laboratory via an in situ oxidative polymerization technique. Their chemical, structural and morphological properties were examined through FESEM, XRD, EDX and FTIR spectroscopic techniques. The electrochemical performance of the as-prepared composites was examined through cyclic voltammogram, electrochemical impedance spectroscopy and galvanostatic charge/discharge measurement techniques. The thermal properties of the as-prepared composites were examined through thermal gravimetric analysis technique. The results obtained were found satisfactory and well suitable for its use as hybrid electrode materials for supercapacitor application.

Keywords $CoCl_2$-doped composites · Cyclic voltammogram · Galvanostatic charge/discharge

Introduction

Electrochemical capacitors (ECs), also called supercapacitors, are the attractive energy storage devices which store energy using either adsorption or fast surface redox reactions [1]. Electrochemical capacitors combined with high-power conventional dielectric capacitors and high specific energy rechargeable batteries show many distinguished advantages such as high power density, high energy

✉ R. B. Choudhary
rbcism@gmail.com

[1] Nanostructured Composite Materials Laboratory, Department of Applied Physics, Indian Institute of Technology (Indian School of Mines), Dhanbad 826004, India

[2] Polymer Research Laboratory, Faculty of Science, University of Malaya, 50603 Kuala Lumpur, Malaysia

density and long cycle life [2–5]. Nowadays, ECs play important role in the development of power sources used in digital communication, hybrid electric vehicles, mobile electronic device, harvesting renewable energy and power backup missiles [6–10]. The fabrication of these electrochemical capacitors involves the employment of lightweight and active chemical ingredients such as conductive polymers and nanoscale inorganic fillers [11]. Conducting polymers are known to have excellent electrochemical properties and are quite inexpensive. The synergistic combination of conductive polymers and inorganic nanofillers also forms the basis of hybrid materials for numerous potential applications in the electrolyte membrane, electromagnetic interference shielding, rechargeable batteries, chemical/biological/gas sensors, anti-corrosion protection coatings, microwave absorption [12–18], organic transistors, organic light-emitting diodes, value-added catalyst and organic solar cells [19–21]. Among these conductive polymers, polyaniline (PANI) is known to be one of the most promising candidates because of its marked electrochemical features and tuneable properties [22]. It is quite inexpensive, highly environment stable, easy to synthesize [23–25] and has high degree of conductivity and high doping/dedoping rate during charge/discharge process [26–28]. It is available in different oxidation forms such as leucoemeraldine base, emeraldine base, pernigraniline base and emeraldine salt. In particular, emeraldine salt is mostly used owing to the reason that it is electrically conductive due to the presence of cation radicals in the polymer (PANI) chain. Due to its high conductivity and net-like structure, PANI has been usually used as a substrate on which metal particles and other metallic oxides can be immobilized [29]. In addition, transition metal oxides are also used as potential electrode materials for supercapacitor application. Their charge storage mechanisms are mainly based on pseudocapacitance [30, 31]. For example, RuO_2 is found to have high capacitance due to its advantageous redox reactions [32], but it has a high cost for elemental Ru which is a major concern for commercial acceptance. Other transition metal oxides such as Co, Ni, Sn, Fe and Mn are comparatively cheap metal oxides. The current trend of research communication emphasizes on the techno-economic development of electrode materials used in supercapacitors with a very high capacity for charge storage and energy density. The reason being that the addition of inorganic fillers cobalt chloride ($CoCl_2$) in the polymeric chain of PANI enables in improving the electrochemical properties. $CoCl_2$ preferably used in the form of hexahydrate ($CoCl_2{\cdot}6H_2O$) is sometimes used as an intriguing chemical ingredient for fabricating the electrode materials of hybrid origin. The addition of $CoCl_2$ into the polymer matrix produces major changes in electrical, dielectric [33], electrochemical and thermal properties. In recent years, a large number of polymeric composite materials with improved electrochemical performance have been studied including MnO_2 nanorods–PANI, graphene–SnO_2-PANI, PANI–zinc acetate–grapheme and PANI–partially exfoliated MWNT [34–36]. Deshmukh et al. [37] are reported to have synthesized PANI–RuO_2 composite through ionic layer adsorption/reaction method and measured its electrochemical properties. They found the specific capacitance value of the order of 664 F/g. Uppugalla et al. [38] reported the heteroatom-doped carbon with PANI composite for supercapacitor application. From the electrochemical performance of CNSO (N, S and O doped carbon)–PANI composite, they observed improved

capacitance value of the order of 372 F/g. Naveen et al. [32] investigated manganese oxide nanorods–PANI composite via single step facile synthesis condition for supercapacitor application. They reported the maximum specific capacitance value of 687 F/g at 5 mV scan rate. In the present communication, we report on the laboratory synthesis of PANI–$CoCl_2$ composite system and its evaluation through cyclic voltammetry (CV), electrochemical impedance spectroscopy (EIS) and constant current charge/discharge (CCD) measurements for their use in supercapacitor application.

Experimental

Materials

Aniline (Merck), hydrochloric acid (Merck), ammonium persulfate (Merck) and cobalt (ll) chloride hexahydrate (Merck) were procured. Acetone (Merck), ethanol (Merck) and many other organic solvents (Merck) were used for the chemical synthesis of $CoCl_2$-doped PANI composites. These chemical reagents were used without any further processing and purification for the chemical synthesis. However, the aniline monomer was distilled twice well before its use throughout the chemical synthesis.

Synthesis

Pure polyaniline was synthesized by the chemical oxidative polymerization process [39] and the product was marked as pure PANI. However, the $CoCl_2$-doped PANI composites were synthesized by the in situ polymerization process. For this purpose, 2 mL aniline was dissolved in 1.5 M HCl mixed with 70 mL distilled water and 10% $CoCl_2$, of cobalt chloride hexahydrate duly dissolved in 5 mL distilled water was added to it. These were properly mixed and vigorously stirred for half an hour. On the other hand, 4 g ammonium persulphate was dissolved in 20 mL of 1.5 M HCl solution, kept for half an hour at 0 °C and then slowly added to the above solution. The solution was constantly stirred at the temperature 0–5 °C. As a consequence, the dark green precipitate was collected on a filter paper and it was successively washed with ethanol, acetone and distilled water, respectively, to remove oligomer, monomer and excess oxidant. Finally, the dark green precipitate was collected and dried under vacuum at 40 °C for 24 h and it was preserved for further studies. The schematic route for the synthesis of $CoCl_2$-doped PANI composites is shown in Fig. 1. Similar composites 15 and 20% $CoCl_2$-doped composites were prepared with $CoCl_2$.

Characterization

Fourier transform infrared (FTIR) spectra were analysed in the wavelength range of 400–4000 cm^{-1} using a thermo-scientific FTIR instrument (Perkin Elmer RXI).

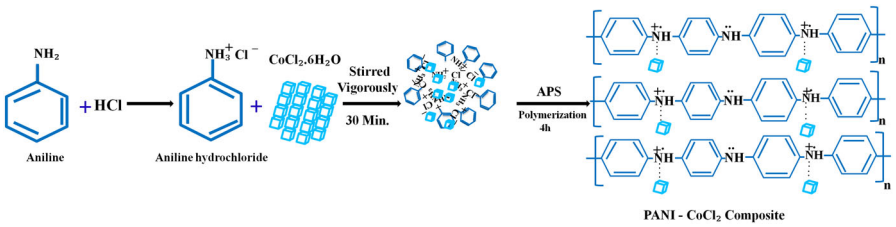

Fig. 1 Schematic route for the synthesis procedure of PANI–$CoCl_2$ composites

For FTIR, KBr was mixed to the material in the ratio of 1:25 in an agate mortar. The phase composition was examined using X-ray diffraction (Model: Rigaku Mini Flex 600) with CuK_α ($\lambda = 1.5406$ Å) radiation in the angular range $2\theta = 10°–90°$. The morphology of $CoCl_2$-doped PANI composite was examined through field effect scanning electron microscope (FESEM Model: ZEISS, Supra 55 Spectrometer). The elemental analyses were examined via energy-dispersive X-ray (EDX) diffraction technique. Thermal gravimetric analysis (TGA) was performed on a thermo-gravimetric analyser SDT model Q600 of TA Instruments Inc., USA. The sample was heated from room temperature to 800 °C using nitrogen flow of 100 mL min^{-1} at the rate of 10 °C min^{-1}. All electrochemical performance, cyclic voltammetry (CV), EIS and galvanostatic charging–discharging (GCD) measurements were carried out by GARMY reference 3000 instruments using a three-electrode system in which composite, Pt and SCE (Ag/AgCl) were working, counter and reference electrodes, respectively. Impedance measurements were performed in the frequency range of 0.1 Hz to 50 kHz at open circuit potential with an ac perturbation of 5 mV. The surface area and the pore size distribution of the as-prepared samples were studied using Quanta Chrome Nova-1000 surface analyser instrument using liquid nitrogen at 77 K. Adsorption–desorption isotherms were recorded to obtain the surface area using the BET method and pore size distribution using the BJH method.

Results and discussion

FTIR analysis

The chemical bond structures for pure PANI, PANI–10% $CoCl_2$, PANI–15% $CoCl_2$ and PANI–20% $CoCl_2$ composites were examined by FTIR spectroscopic technique. Figure 2 shows the FTIR spectra for pure PANI, PANI–10% $CoCl_2$, PANI–15% $CoCl_2$ and PANI–20% $CoCl_2$ composites and their characteristic peaks have been depicted in Table 1. The FTIR spectra for pure PANI showed characteristic peaks at 596, 811, 1147, 1240, 1305, 1493 and 1573 cm^{-1}, respectively. The peak 811 cm^{-1} corresponded to the out-of-plane bending C–H

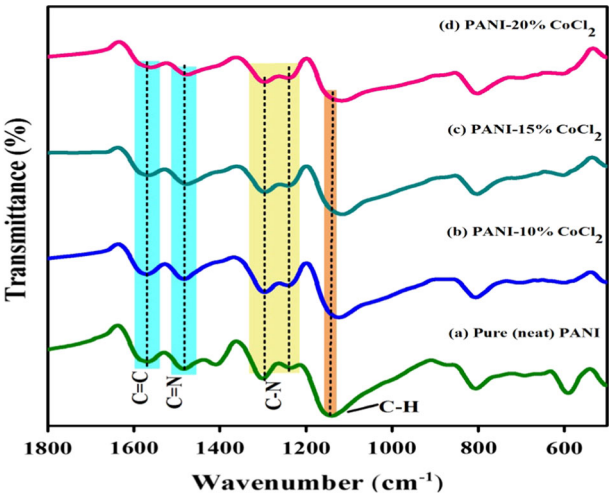

Fig. 2 FTIR spectra for **a** pure PANI, **b** PANI–10% $CoCl_2$, **c** PANI–15% $CoCl_2$, and **d** PANI–20% $CoCl_2$ composites

Table 1 FTIR characteristic peaks for pure PANI, PANI–10% $CoCl_2$, PANI–15% $CoCl_2$ and PANI–20% $CoCl_2$ composites

FTIR characteristic Band assignments	Wavenumbers (cm^{-1}) for PANI and $CoCl_2$-doped PANI composites			
	Pure PANI	PANI–10% $CoCl_2$	PANI–15% $CoCl_2$	PANI–20% $CoCl_2$
C–H stretching vibration	811	791	791	791
C–N stretching vibration	1240	1238	1238	1238
C=C stretching vibration	1573	1573	1573	1573
C=N stretching vibration	1493	1472	1472	1472
C–N stretching vibration	1305	1294	1294	1294

vibrations of the 1,4-substituted benzene ring [40]. The peak at 1147 cm^{-1} was assigned to plane deformation vibrations of the C–H bond. The peak at 596 cm^{-1} was due to out-of-plane bending of the C–H bond in the aromatic ring. The band at 1240 cm^{-1} was assigned to stretching vibration of C–N in the benzenoid ring. The bands at 1573 and 1493 cm^{-1} corresponded to the C=C stretching vibration of the quinoid ring and the C=N stretching vibration of the benzenoid unit, respectively [41, 42]. The peaks at 1240 and 1305 cm^{-1} were attributed to the C–N stretching vibrations with oxidation or protonation states in PANI [43]. However, For PANI–10% $CoCl_2$, PANI–15% $CoCl_2$ and PANI–20% $CoCl_2$ composites, the band at 1294 cm^{-1} was assigned to the C–N stretching vibration. This band shifted by 10 cm^{-1} (1305–1294 cm^{-1}) when $CoCl_2$ was added to the reaction system. This indicated that Co^{2+} ions interacted with the nitrogen atoms in the polymeric chain of the as-prepared composites.

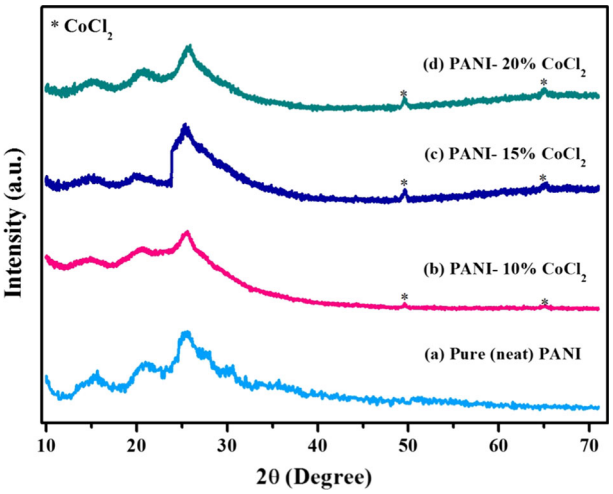

Fig. 3 XRD spectra for **a** pure PANI, **b** PANI–10% $CoCl_2$, **c** PANI–15% $CoCl_2$, and **d** PANI–20% $CoCl_2$ composites

XRD analysis

Figure 3 shows the X-ray diffraction patterns for pure PANI, PANI–10% $CoCl_2$, PANI–15% $CoCl_2$ and PANI–20% $CoCl_2$ composites. The XRD pattern for pure PANI showed three diffraction peaks centered at 15.0°, 20.3° and 25.4°, respectively [44]. This occurred due to scattering of the PANI chains at interplanar spacing. From the XRD spectra, the co-existence of pure PANI and $CoCl_2$ particles in the composites was observed. The characteristic peaks revealed semi-crystalline behavior of pure PANI, PANI–10% $CoCl_2$, PANI–15% $CoCl_2$ and PANI–20% $CoCl_2$ composites. The peaks for PANI–10% $CoCl_2$, PANI–15% $CoCl_2$ and PANI–20% $CoCl_2$ composites were observed at 2θ values of 49.66° and 64.92°. The 2θ values for composites were nearly the same as in the literature reported by Gupta et al. [40].

FESEM analysis

The morphological behaviour of pure PANI, PANI–10% $CoCl_2$, PANI–15% $CoCl_2$ and PANI–20% $CoCl_2$ composites has been shown in Fig. 4. Figure 4 reveals that the morphology of PANI–10% $CoCl_2$, PANI–15% $CoCl_2$ and PANI–20% $CoCl_2$ composites were spherical in nature. This morphology was probably due to the reason that one Co^{2+} ion interacted with more than one nitrogen atom in the PANI chain. The specific capacitance of pure PANI and PANI–$CoCl_2$ composites depends on the surface area as well as on its porosity [45]. The synergistic effect of capacitance has been markedly enhanced in PANI–10% $CoCl_2$ composite as compared to that of pure PANI, PANI–15% $CoCl_2$ and PANI–20% $CoCl_2$ composites. Figure 5 shows the EDX spectra for pure PANI, PANI–10% $CoCl_2$, PANI–15% $CoCl_2$ and PANI–20% $CoCl_2$ composites and indicates the element

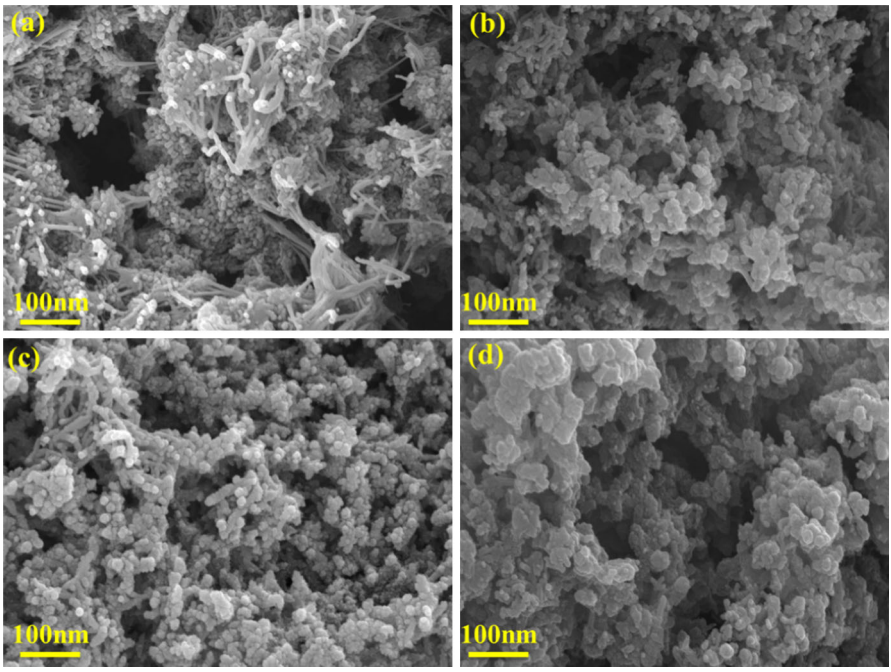

Fig. 4 FESEM images for **a** pure PANI, **b** PANI–10% $CoCl_2$, **c** PANI–15% $CoCl_2$, and **d** PANI–20% $CoCl_2$ composites

presence of Cl, N, C, S and Co in it. A trace amount of platinum (pt) was also observed due to the platinum coating of the samples.

Brunauer–Emmett–Teller (BET) analysis

The as-prepared samples were further characterized with nitrogen (N_2) absorption–desorption and the corresponding results are depicted in Fig. 6. The surface area measurement and pore sized distribution of pure PANI, PANI–10% $CoCl_2$, PANI–15% $CoCl_2$ and PANI–20% $CoCl_2$ are shown in Fig. 6a, b, respectively. The surface area value for pure PANI was found to be 11.57 $m^2\ g^{-1}$. The isotherms were witnessed to be of type IV suggesting the mesoporous nature of the samples. The surface area was found to be 41 $m^2\ g^{-1}$ for PANI–10% $CoCl_2$. In the case of PANI–15% $CoCl_2$, the surface area decreased to 39 $m^2\ g^{-1}$. With a further increase in the content of $CoCl_2$ the surface area was enhanced and reached a value of 58 $m^2\ g^{-1}$. The observed values of specific capacitances were in accordance with the observed porosity and the obtained surface area of the samples. An enhanced surface area for the sample resulted in an increased specific capacitance. This could be attributed to the formation of interconnected pores resulting in the formation of an easy pathway for charge transfer, thereby increasing the specific capacitance of the sample.

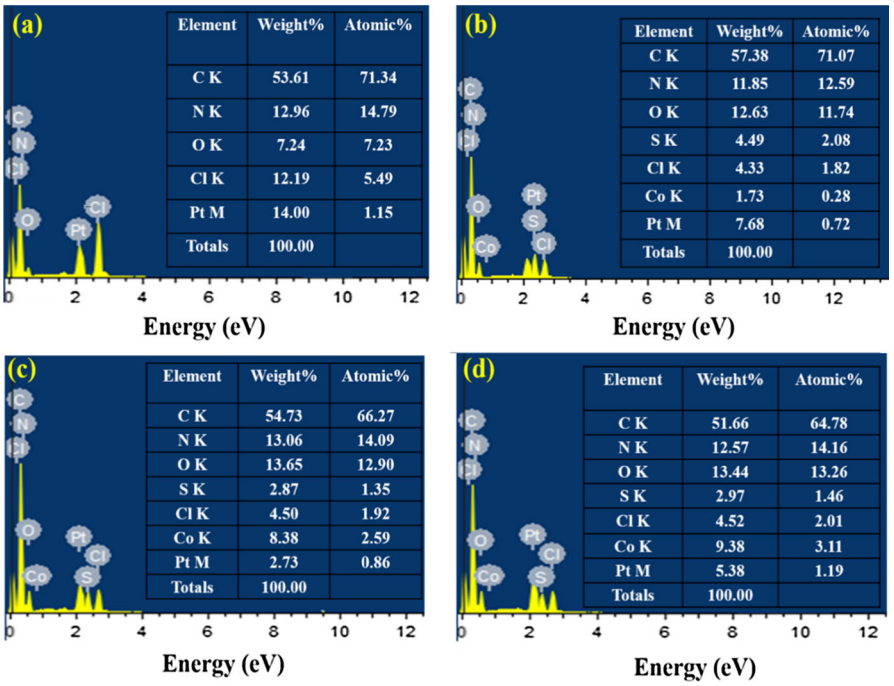

Fig. 5 EDX spectra for **a** pure PANI, **b** PANI–10% $CoCl_2$, **c** PANI–15% $CoCl_2$ and **d** PANI–20% $CoCl_2$ composites

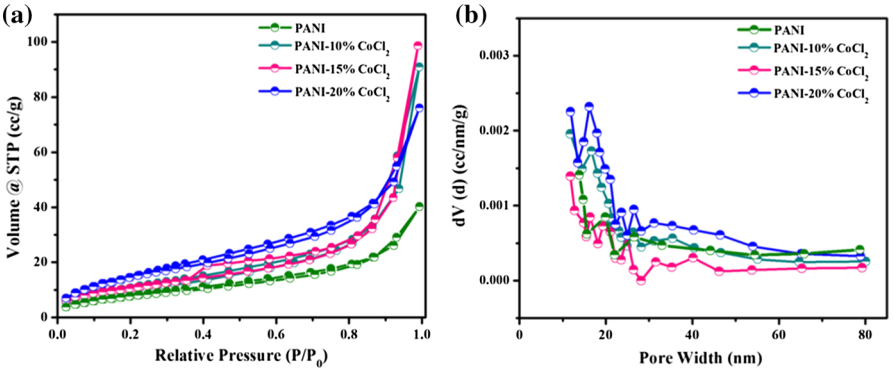

Fig. 6 **a** BET surface area, and **b** pore size distribution of all polymeric composites

Electrochemical measurements

The CV measurement technique was employed to examine the electrochemical performance of PANI–$CoCl_2$ composite electrode material as shown in Fig. 7. The pure PANI, PANI–10% $CoCl_2$, PANI–15% $CoCl_2$ and PANI–20% $CoCl_2$ composites were evaluated for the capacitive performance comparison of PANI

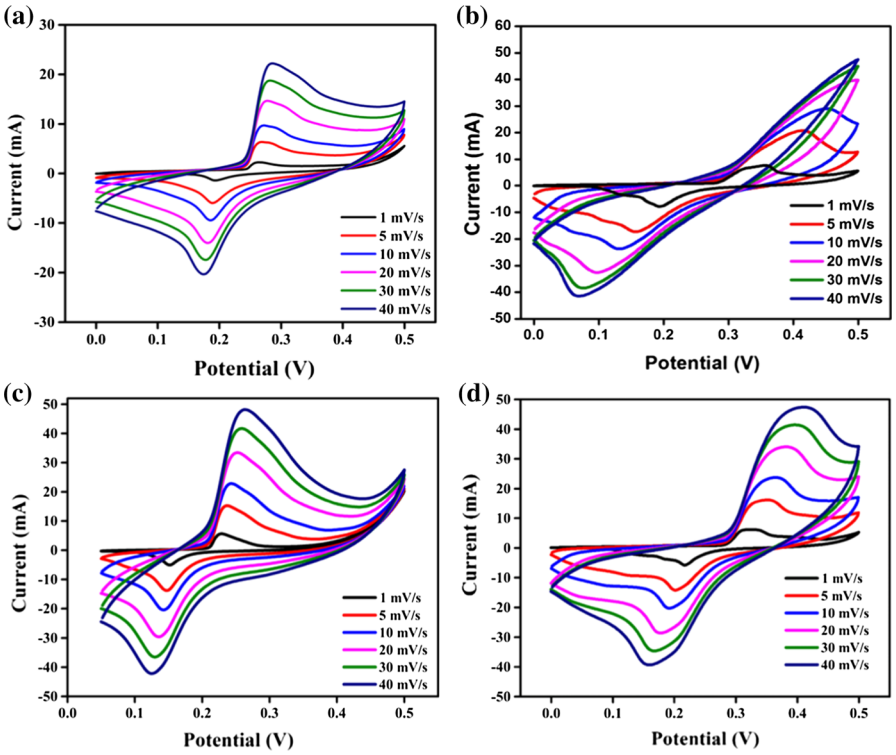

Fig. 7 CV curves for **a** pure PANI, **b** PANI–10% $CoCl_2$, **c** PANI–15% $CoCl_2$ and **d** PANI–20% $CoCl_2$ composites at varying scan rates

after the addition of $CoCl_2$. The CV measurement was performed in the potential window 0.05–0.5 V (Ag/AgCl) using 1 M KOH electrolyte. Figure 7a–d illustrates the CV curves for pure PANI, PANI–10% $CoCl_2$, PANI–15% $CoCl_2$ and PANI–20% $CoCl_2$ composite electrodes at various scan rates ranging from 1 to 40 mV/s. All the CV curves exhibited redox peaks implying that its capacitance was derived from pseudocapacitive behaviour due to the presence of reversible Faradaic redox reactions. It was observed that with the increase in scan rate, the anodic and cathodic peaks shifted towards the positive and negative sides, respectively, and currents were found to be increased. In the case of PANI–10% $CoCl_2$, the peak intensity decreased due to the effect of $CoCl_2$. The PANI–10% $CoCl_2$ showed large current response and larger integrated area as compared to other samples. This was probably due to the strengthened electric polarization and the possible kinetic irreversibility of electrolyte ions at the electrode surface [46].

The specific capacitance of the electrodes was calculated from the results based on the CV measurements using the following equation:

$$C_S = \frac{1}{vm\Delta V_{if}} \int_{Vi}^{Vf} I \times V dV, \quad (1)$$

where C_s—specific capacitance (F/g), v—scan rate (V/s), m—a mass of the active material (g) and ΔV_{if}—applied potential window. The integral term of Eq. (1) is equal to the area under the CV curve. The calculated values of specific capacitance (C_s) for pure PANI, PANI–10% $CoCl_2$, PANI–15% $CoCl_2$ and PANI–20% $CoCl_2$ composites were found 382, 918, 481 and 713 F/g (shown in Table 2), respectively, at a scan rate of 1 mV/s. Figure 7 shows that PANI–10% $CoCl_2$ represented the higher value of specific capacitance than that of pure PANI, PANI–15% $CoCl_2$ and PANI–20% $CoCl_2$ composites at all the scan rates. This enhancement in specific capacitance (C_s) of PANI–10% $CoCl_2$ was attributed to the optimum presence of metal salt [47] inside the polymeric composite.

The charge–discharge behaviours for pure PANI, PANI–10% $CoCl_2$, PANI–15% $CoCl_2$ and PANI–20% $CoCl_2$ composites have been shown in Fig. 8. The galvanostatic charge/discharge curves for the pure PANI, PANI–10% $CoCl_2$, PANI–15% $CoCl_2$ and PANI–20% $CoCl_2$ composites in 1 M KOH solution were carried out at a current density of 0.5, 1 and 2 A/g, respectively. As illustrated in Fig. 8a–d, all electrode materials showed nonlinear discharge curves which indicated the pseudocapacitive behaviour of inorganic filler. This resulted from the electrochemical adsorption–desorption phenomena of redox reaction at the electrode/electrolyte interface. In addition, it can be seen that the charging/discharging time decreased with the increase in current density from 0.5 to 2A/g. This could be explained in terms of the fact that at low current density, OH^- had sufficient time to diffuse into the available sites at the electrode material. However, at high current density, OH^- can only approach the outer surface of the electrode materials [48]. Moreover, the discharge time for PANI–10% $CoCl_2$ was significantly increased by incorporation of $CoCl_2$ as compared to pure PANI and it was also higher than other composites, indicating that efficient ion or charge transfer occurred in PANI–10% $CoCl_2$. The PANI–10% $CoCl_2$ composite shows higher specific capacitance due to high surface area value 41 m^2g^{-1} and high thermal stability as shown in the BET analysis and Fig. 10, respectively.

EIS measurements

Electrochemical impedance spectroscopic (EIS) technique was employed to measure the internal resistance, charge transfer kinetics and ion diffusion process

Table 2 Estimated values for specific capacitance from CV curves at 1 mv/s scan rate

Scan rate (mv/s)	Specific capacitance (F/g) for polymeric samples			
	Pure PANI	PANI–10% $CoCl_2$	PANI–15% $CoCl_2$	PANI–20% $CoCl_2$
1	382	918	481	713

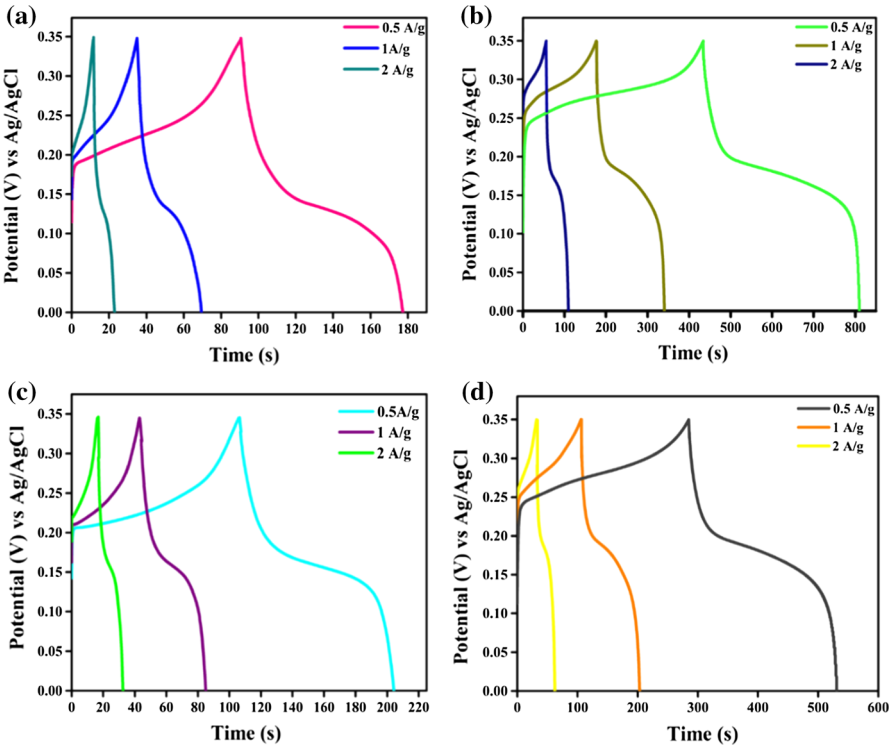

Fig. 8 Galvanostatic CD curves for **a** Pure PANI, **b** PANI–10% $CoCl_2$, **c** PANI–15% $CoCl_2$ and **d** PANI–20% $CoCl_2$ composites at varying current densities

of the electrode materials as shown in Fig. 9. Figure 9 shows EIS plots (Nyquist plot) between Z′ and Z″ recorded in the frequency range 1 Hz–100 kHz. The ESR values for pure PANI, PANI–10% $CoCl_2$, PANI–15% $CoCl_2$ and PANI–20% $CoCl_2$ composites obtained from the intersection of the Nyquist plot at the *X*-axis were 3.14, 1.78, 0.86 and 0.97 Ω, respectively. The smaller value of ESR for pure PANI, PANI–10% $CoCl_2$, PANI–15% $CoCl_2$ and PANI–20% $CoCl_2$ composites suggested the decreased charge transfer resistance between the electrolyte solution and the interface of the sample [49]. In addition, for pure PANI, PANI–10% $CoCl_2$, PANI–15% $CoCl_2$ and PANI–20% $CoCl_2$ composites showed a semicircle in the higher frequency range, followed by a line in a lower frequency. The diameter of the semicircle estimated the Faradaic charge transfer resistance (R_{ct}) related to the surface area and electrical conductivity of the electrode material, whereas the straight line observed in the lower frequency range showed the characteristic of Warburg impedance which measured diffusion resistance offered by the materials. As seen in Fig. 9, the slope for PANI–10% $CoCl_2$ was larger than that of the pure PANI, PANI–15% $CoCl_2$ and PANI–20% $CoCl_2$ composites, implying a lower internal resistance leading to a higher conductivity. Thus, the above results showed that PANI–10% $CoCl_2$ composite elucidated overall better electrochemical performance in terms of CV, GCD and EIS measurements as compared to that of

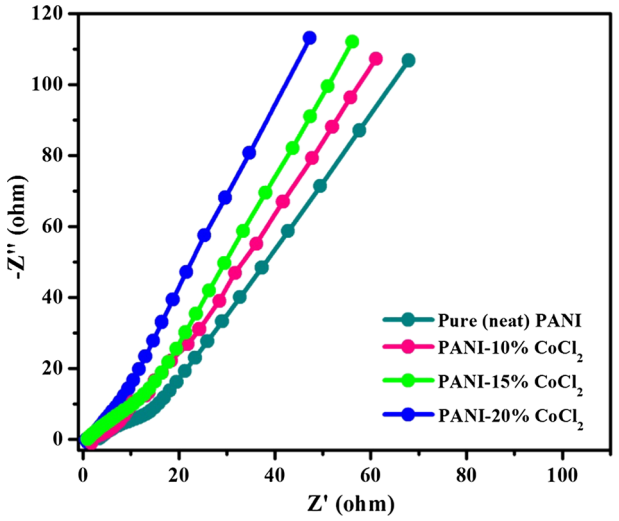

Fig. 9 Nyquist plots for pure PANI, PANI–10% $CoCl_2$, PANI–15% $CoCl_2$ and PANI–20% $CoCl_2$ composites

pure PANI, PANI–15% $CoCl_2$ and PANI–20% $CoCl_2$ composites, since the capacitance of the electrode material depends on the porosity as well as on the specific surface area. Further, the polyaniline (PANI) chains have a higher porosity as shown in the FESEM image (Fig. 4a). Nonetheless, the amount of polyaniline decreases in PANI–15% $CoCl_2$ and PANI–20% $CoCl_2$ composites. Therefore, the capacitance values for PANI–10% $CoCl_2$ composite exceeds in comparison to PANI–15% $CoCl_2$ and PANI–20% $CoCl_2$ composites. Hence, PANI–10% $CoCl_2$ composite represents an optimum and synergistic combination of the polymeric matrix of the PANI–$CoCl_2$ composite. The above results stand valid also from the TGA study in which PANI–10% $CoCl_2$ composite showed the highest thermal stability in comparison to PANI–15% $CoCl_2$ and PANI–20% $CoCl_2$ composites as shown in Fig. 10.

Thermal properties

Figure 10 represents the TGA thermograms for pure PANI, PANI–10% $CoCl_2$, PANI–15% $CoCl_2$ and PANI–20% $CoCl_2$ composites. It showed that for pure PANI, a three-step thermal decomposition occurred followed by respective weight loss. The first stage decomposition occurred up to temperature 150 °C due to loss of moisture. The second stage decomposition occurred in the temperature range 200–300 °C due to dopant anion present in the polymer. The third decomposition stage occurred between temperatures 300 and 800 °C due to the decomposition of the molecular chain of polyaniline (PANI). The trend of thermal decomposition and mass loss of PANI–10% $CoCl_2$, PANI–15% $CoCl_2$ and PANI–20% $CoCl_2$ composites were similar to that of the pure PANI. However, the thermal stability of the composites was higher than that of the said pure PANI. The degradation

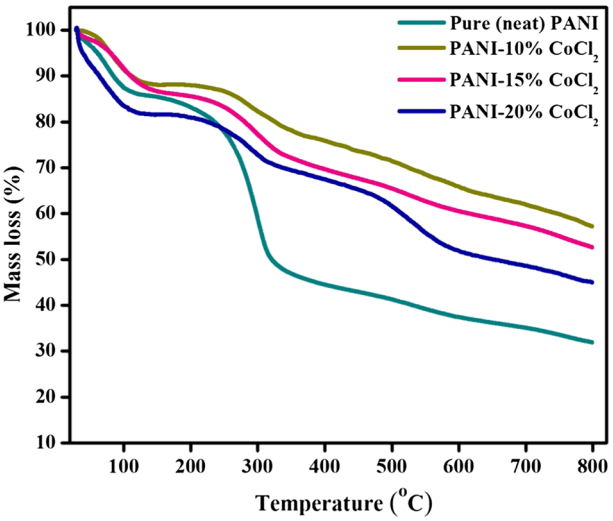

Fig. 10 TGA curves for pure PANI, PANI–10% $CoCl_2$, PANI–15% $CoCl_2$ and PANI–20% $CoCl_2$ composites

temperatures for pure PANI, PANI–10% $CoCl_2$, PANI–15% $CoCl_2$ and PANI–20% $CoCl_2$ composites are shown in Table 3. It was clearly seen that the thermal stability of the composites decreased on increasing the concentration of $CoCl_2$ particlesm, because the thermal degradation process starts at a lower temperature. This result was attributed to the removal of dopants [50].

Conclusion

PANI–$CoCl_2$ composites were successfully synthesized in the laboratory via an in situ polymerization process. The FTIR study explained the chemical bond structures of backbone chains for pure PANI, PANI–10% $CoCl_2$, PANI–15% $CoCl_2$ and PANI–20% $CoCl_2$ composites. The XRD study explained the semi-crystalline behaviour of pure PANI, PANI–10% $CoCl_2$, PANI–15% $CoCl_2$ and PANI–20%

Table 3 Degradation temperature for pure PANI, PANI–10% $CoCl_2$, PANI–15% $CoCl_2$ and PANI–20% $CoCl_2$ composites

Polymeric samples	Temperature range (°C) for 1st degradation	Temperature range (°C) for 2nd degradation	Temperature range (°C) for 3rd degradation	Residual weight % at 800 °C
Pure (neat) PANI	14.14	43.92	3.48	31.95
PANI–10% $CoCl_2$	13.32	13.01	7.98	57.27
PANI–15% $CoCl_2$	14.22	15.45	12.51	52.67
PANI–20% $CoCl_2$	18.36	14.66	15.10	44.98

$CoCl_2$ composites. The FESEM study explained the spherical morphology of the as-prepared composites. The cyclic voltammetry (CV) measurement showed that PANI–10% $CoCl_2$ composite exhibited highly enhanced specific capacitance value (918 F/g) as compared to pure PANI (382 F/g), PANI–15% $CoCl_2$ (481 F/g) and PANI–20% $CoCl_2$ (713 F/g) composites at the scan rate $\sim$ 1 mV/s. Such an intriguing electrochemical performance was attributed to the optimum synergistic properties of the combined capacitive contribution from the inorganic filler ($CoCl_2$) as well as the polymer (PANI). Finally, the TGA study explained that PANI–10% $CoCl_2$ composite imparted the highest thermal stability.

Acknowledgements The authors express their sincere thanks to Professor (Dr.) D. C. Panigrahi, Director Indian Institute of Technology (ISM) Dhanbad, India, for his constant encouragement in this communication.

References

1. Simon P, Gogotsi Y (2008) Materials for electrochemical capacitors. Nat Mater 7:845–854
2. Wei TY, Chen CH, Chien HC, Lu SY, Hu CC (2010) A cost-effective supercapacitor material of ultrahigh specific capacitances: spinel nickel cobaltite aerogels from an epoxide-driven sol–gel process. Adv Mater 22:347–351
3. Fan Z, Yan J, Wei T, Zhi L, Ning G, Li T, Wei F (2011) Asymmetric supercapacitors based on graphene/MnO2 and activated carbon nanofiber electrodes with high power and energy density. Adv Funct Mater 21:2366–2375
4. Liu C, Li F, Ma L, Cheng H (2010) Advanced materials for energy storage. Adv Mater 22:E28–E62
5. Stoller MD, Park SJ, Zhu Y, An J, Ruoff RS (2008) Graphene-based ultracapacitors. Nano Lett 8:3498–3502
6. Conway BE (1999) Electrochemical supercapacitors scientific fundamentals and technological applications. Springer Science Business Media, Berlin. doi:10.1007/978-1-4757-3058-6
7. Tian W, Wang X, Zhi C, Zhai T, Liu D, Zhang C, Golberg D, Bando Y (2013) Ni $(OH)_2$ nanosheet @ Fe_2O_3 nanowire hybrid composite arrays for high-performance supercapacitor electrodes. Nano Energy 2:754–763
8. Zhi J, Deng S, Zhang Y, Wang Y, Hu A (2013) Embedding Co_3O_4 nanoparticles in SBA-15 supported carbon nanomembrane for advanced supercapacitor materials. J Mater Chem A 1:3171–3176
9. Nethravathi C, Rajamathi CR, Rajamathi M, Wang X, Gautam UK, Golberg D, Bando Y (2014) Cobalt hydroxide/oxide hexagonal ring-graphene hybrids through chemical etching of metal hydroxide platelets by graphene oxide: energy storage application. ACS Nano 8:2755–2765
10. Salunkhe RR, Jang K, Lee S, Ahn H (2012) Aligned nickel-cobalt hydroxide nanorod arrays for electrochemical pseudocapacitor applications. RSC Adv 2:3190–3193
11. Thakur AK, Choudhary RB (2016) High-performance supercapacitors based on polymeric binary composites of polythiophene (PTP)–titanium dioxide (TiO_2). Synth Met 220:25–33
12. Thakur AK, Choudhary RB, Majumder M, Gupta G, Shelke MV (2016) Enhanced electrochemical performance of polypyrrole coated MoS_2 composites as electrode material for supercapacitor application. J Electr Chem 782:278–287
13. Makela T, Pienimaa S, Taka T, Jussila S, Isotalo H (1997) Thin polyaniline films in EMI shielding. Synth Met 85:1335–1336
14. Kuwabata S, Masui S, Yoneyama H (1999) Charge–discharge properties of composites of $LiMn_2O_4$ and polypyrrole as positive electrode materials for 4 V class of rechargeable Li batteries. Electrochim Acta 44:4593–4600
15. Lee I, Luo X, Huang J, Cui XT, Yun M (2012) Detection of cardiac biomarkers using single polyaniline nanowire-based conductometric biosensors. Biosenor 2:205–220
16. Wojkiewicz JL, Bliznyuk VN, Carquigny S, Elkamchi N, Redon N, Lasri T, Pud AA, Reynaud S (2011) Nanostructured polyaniline-based composites for ppb range ammonia sensing. Sensor Actuator b-Chem 160:1394–1403

17. Mirmohseni A, Oladegaragoze A (2000) Anticorrosive properties of polyaniline coating on iron. Synth Met 114:105–108
18. Rose TL, Antonio SD, Jillson MH, Kron AB, Suresh R, Wang F (1997) A microwave shutter using conductive polymers. Synth Met 85:1439–1440
19. Kaune G, Ruderer MA, Metwalli E, Wang W, Couet S, Schlage K, Röhlsberger R, Roth SV, Müller-Buschbaum P (2009) *In-situ* GISAXS study of gold film growth on conducting polymer films. ACS Appl Mater Interfaces 1:353–360
20. Ruffino F, Torrisi V, Marletta G, Grimaldi MG (2011) Growth morphology of nanoscale sputter-deposited Au films on amorphous soft polymeric substrates. Appl Phys A 103:939–949
21. Wu JL, Chen FC, Hsiao YS, Chien FC, Chen P, Kuo CH, Huang MH, Hsu CS (2011) Surface plasmonic effects of metallic nanoparticles on the performance of polymer bulk heterojunction solar cells. ACS Nano 5:959–967
22. Heeger AJ (2001) Nobel lecture: semiconducting and metallic polymers: the fourth generation of polymeric materials. J Rev Mod Phy 73:681–700
23. Kaiser AB (2001) Systematic conductivity behavior in conducting polymers: effects of heterogeneous disorder. Adv Mater 13:927–941
24. Tang Q, Wu J, Sun H, Lin J, Fan S, Hu D (2008) Polyaniline/polyacrylamide conducting composite hydrogel with a porous structure. Carbohydr Polym 74:215–219
25. Ping Z, Nauer GE, Neugebauer H, Theiner J, Neckel A (1997) Protonation and electrochemical redox doping processes of polyaniline in aqueous solutions: investigations using in situ FTIR-ATR spectroscopy and a new doping system. J Chem Soc Faraday Trans 93:121–129
26. Wang H, Lin J, Shen ZX (2016) Polyaniline based electrode materials for energy storage and conversion. J Sci Adv Mater Devices 1:225–255
27. Gupta V, Miura N (2005) Electrochemically deposited polyaniline nanowire's network a high-performance electrode material for redox supercapacitor. Electrochem Solid State Lett 8:A630–A632
28. Ding KQ (2009) Cyclic voltammetrically prepared MnO_2-polyaniline composite and its electrocatalysis for oxygen reduction reaction (ORR). J Chin Chem Soc 56:891–897
29. Chen PC, Shen G, Shi Y, Chen H, Zhou C (2010) Preparation and characterization of flexible asymmetric supercapacitors based on transition-metal-oxide nanowire/single-walled carbon nanotube hybrid thin-film electrodes. ACS Nano 4:4403–4411
30. Zhang J, Ma J, Zhang LL, Guo P, Jiang J, Zhao XS (2010) Template synthesis of tubular ruthenium oxides for supercapacitor applications. J Phys Chem C 114:13608–13613
31. Gujar TP, Kim WY, Puspitasari I, Jung KD, Joo OS (2007) electrochemically deposited nanograin ruthenium oxide as a pseudocapacitive electrode. Int J Electrochem Sci 2:666–673
32. Naveen AN, Selladurai (2015) Fabrication and performance evaluation of symmetrical supercapacitor based on manganese oxide nanorods—PANI composite. Mater Sci Semicon Process 40:468–478
33. Majhi M, Choudhary RB, Maji P (2015) $CoCl_2$ reinforced polymeric nanocomposites of conjugated polymer (polyaniline) and its conductive properties. Bull Mater Sci 38:1195–1203
34. Jin Y, Jia M (2015) Design and synthesis of nanostructured graphene-SnO_2-polyaniline ternary composite and their excellent supercapacitor performance. Colloid Surface A 464:17–25
35. Das AK, Maiti S, Khatua BB (2015) High performance electrode material prepared through in situ polymerization of aniline in the presence of Zinc acetate and grapheme nanoplatelets for supercapacitor applicaton. J Electroanal Chem 739:10–19
36. Darshna DP, Sivaraman P, Sarada PM, Manoranjan P (2015) Polyaniline/partially exfoliated multi-walled carbon nanotubes based nanocomposites for supercapacitors. Electrochim Acta 155:402–410
37. Deshmukh PR, Patil SV, Sartale SD, Lokhande CD (2014) Inexpensive synthesis route of porous polyaniline–ruthenium oxide composite for supercapacitor application. Chem Engg J 257:82–89
38. Uppugalla S, Male U, Srinivasan P (2014) Design and synthesis of heteroatoms doped carbon/polyaniline hybrid material for high performance electrode in supercapacitor application. Electrochim Acta 146:242–248
39. Stejskal J, Gilbert RG (2002) Polyaniline, preparation of a conducting polymer. Pure Appl Chem 74:857–867
40. Gupta K, Chakraborty G, Ghatak S, Jana PC, Meikap AK (2010) Synthesis of copper chloride and cobalt chloride doped polyanilines and their magnetic and alternating-current transport properties. J Appl Polym Sci 115:2911–2917
41. Patil R, Roy AS, Anilkumar KR, Prasad MVNA, Ekhelikar S (2011) Electrical conductivity of polyaniline/$NiZnO_3$ composites: a solid state electrolyte. Ferroelectrics 423:77–85

42. Khairy M, Gouda ME (2015) Electrical and optical properties of Nickel ferrite/polyaniline nanocomposites. J Adv Res 6:555–562
43. Quillard S, Louran G, Lefrant S, Macdiarmid AG (1994) Vibrational analysis of polyaniline: a comparative study of leucoemeraldine, emeraldine, and pernigraniline bases. Phys Rev B 50:12496–12508
44. Mohamed MB, Sayed KEL (2014) Structural, magnetic and dielectric properties of (PANI)—$Ni_{0.5}Zn_{0.5}Fe_{1.5}C_{0.5}O_4$ nanocomposite. Compos Part B. 56:270–278
45. Sahoo S, Karthikeyan G, Nayak GCh, Das CK (2011) Electrochemical characterization of in situ polypyrrole coated graphene nanocomposites. Synth Met 161:1713–1719
46. Jahromi SP, Pandikumar A, Goh BT, Lim YS, Basirun WJ, Lim HN, Huang NM (2015) Influence of particle size on performance of a nickel oxide nanoparticle-based supercapacitor. RSC Adv 5:14010–14019
47. Maiti S, Khatua BB (2013) Electrochemical and electrical performances of cobalt chloride ($CoCl_2$) doped polyaniline (PANI)/graphene nanoplate (GNP) composite. RSC Adv 3:12874–12885
48. Shi X, Zhu J, Zhang Y, He S, Bi Y, Zhang L (2015) Facile synthesis of structure-controllable, N-doped graphene aerogels and their application in supercapacitors. RSC Adv 5:77130–77137
49. Khandanlou R, Ahmad MB, Shameli K, Saki E, Kalantari K (2014) Studies on properties of rice straw/polymer nanocomposites based on polycaprolactone and Fe_3O_4 nanoparticles and evaluation of antibacterial activity. Int J Mol Sci 15:18466–18483
50. Han G, Liu Y, Zhang L, Kan E, Zhang S, Tang J, Tang W (2014) MnO_2 nanorods intercalating graphene oxide/polyaniline ternary composites for robust high-performance supercapacitors. Sci Rep 4:4824